Magnetic catalysis and inverse catalysis for heavy pions

G. Endrődi,[a] **M. Giordano,**[b] **S.D. Katz,**[b] **T.G. Kovács**[b,c] **and F. Pittler**[d]

[a]*Institute for Theoretical Physics, Goethe Universität Frankfurt,*
D-60438 Frankfurt am Main, Germany

[b]*ELTE Eötvös Loránd University, Institute for Theoretical Physics,*
Pázmány P.s. 1/A, H-1117, Budapest, Hungary

[c]*Institute for Nuclear Research of the Hungarian Academy of Sciences,*
Bem tér 18/c, H-4026 Debrecen, Hungary

[d]*HISKP(Theory), University of Bonn,*
Nussallee 14-16, D-53115 Bonn, Germany

E-mail: endrodi@th.physik.uni-frankfurt.de, giordano@bodri.elte.hu,
katz@bodri.elte.hu, kgt@atomki.mta.hu, pittler@hiskp.uni-bonn.de

Abstract: We investigate the QCD phase diagram for nonzero background magnetic fields using first-principles lattice simulations. At the physical point (in terms of quark masses), the thermodynamics of this system is controlled by two opposing effects: magnetic catalysis (enhancement of the quark condensate) at low temperature and inverse magnetic catalysis (reduction of the condensate) in the transition region. While the former is known to be robust and independent of the details of the interactions, inverse catalysis arises as a result of a delicate competition, effective only for light quarks. By performing simulations at different quark masses, we determine the pion mass above which inverse catalysis does not take place in the transition region anymore. Even for pions heavier than this limiting value — where the quark condensate undergoes magnetic catalysis — our results are consistent with the notion that the transition temperature is reduced by the magnetic field. These findings will be useful to guide low-energy models and effective theories of QCD.

Contents

1 Introduction

Strongly interacting matter at finite temperature in the presence of external magnetic fields has been the subject of intense research in recent years (see, e.g., refs. [1–4] for recent reviews). Besides physical applications in the study of heavy ion collisions, neutron stars, and the early Universe, this topic is of considerable interest for a better theoretical understanding of Quantum Chromodynamics (QCD) in the presence of external sources. In this respect, nonperturbative studies by means of numerical calculations on the lattice have shown a richer variety of effects than initially expected. Perturbative and model calculations led one to expect that, regardless of the temperature, one would find an increase of the quark condensate as the magnitude B of the magnetic field was increased, a phenomenon called *magnetic catalysis* (MC) [5], and a corresponding increase of the (pseudo)critical temperature T_c. This was initially confirmed by lattice studies [6], but the situation changed as the numerical calculations were made more precise. For physical quark masses and on fine lattices, it turned out that while MC is displayed away from the critical region, near T_c the quark condensate decreases with B, i.e., *inverse magnetic catalysis* (IMC) is found, and correspondingly T_c decreases [7, 8]. This behavior, originally observed for $B < 1$ GeV^2, was later found to persist for stronger magnetic fields and it was argued that $T_c(B)$ monotonically decreases up to asymptotically large magnetic fields [9]. Results supporting IMC were also obtained by further lattice simulations [10–12]. It was then believed that MC and IMC corresponded to T_c being respectively an increasing or decreasing function of B, but a recent study has shown that as the pion mass is increased, the behavior near T_c crosses over from IMC to MC, while T_c remains a decreasing function of B all along [13].

On the theoretical side, a full understanding of the microscopic mechanism responsible for these effects is still lacking. In this respect, it is useful to recall, following refs. [14, 15], that the magnetic field enters the calculation of the condensate both directly through the observable, and indirectly through the fermion determinant contributing to the weight of

the gauge configurations. The corresponding effects are called *valence effect* and *sea effect*, respectively. As a matter of fact, the magnetic field has a catalytic effect on the spectrum of the Dirac operator in a given gauge configuration, increasing the density of low modes and therefore the condensate. The valence effect therefore always acts in the direction of MC: in particular, the valence condensate, obtained by averaging over configurations with $B = 0$ in the fermionic determinant, increases with B at all temperatures. When reweighting the valence condensate to the full one, including a nonzero B in the determinant, those configurations with a larger change in the spectral density near the origin will be suppressed more: this is the sea effect, which is expected to act in the direction of IMC. In the end, it is the balance between the two effects that determines whether MC or IMC will take place. Since the magnetic field couples to the gauge field only indirectly through the fermionic determinant, it is the sea effect which is responsible for the observed changes in the confining properties of the theory — like the Polyakov loop expectation value [15] or the static quark-antiquark potential [16].

It is clear from the discussion above that there are two main issues that need to be clarified to fully explain the effect of an external magnetic field in QCD. The first issue is the detailed mechanism that leads to an enhanced density of low modes of the Dirac operator when B is nonzero. While for free quarks the degeneracy of the Landau levels is responsible for this enhancement [17], in strongly interacting QCD these levels are in general not well defined anymore. Remarkably, the lowest Landau level can still be meaningfully identified and was shown to quantitatively explain the increase of the quark condensate for strong magnetic fields on the lattice [18].

The second issue is the delicate balance between the catalytic drive of the valence effect and the anticatalytic drive of the sea effect. This amounts to investigating the circumstances under which IMC is realized around the transition temperature. This is particularly relevant for the interpretation of the IMC phenomenon. Recently, a multitude of low-energy models and effective theories have been employed to explain the lattice findings about IMC (see, e.g., refs. [19–39]). In most of these settings magnetic catalysis arises naturally, but to reproduce inverse catalysis around T_c turned out to require a tuning of model parameters as functions of the magnetic field (see, e.g., refs. [40–43]). In several cases such a reparameterization only sufficed to achieve a reduction in $T_c(B)$ for low magnetic fields, whereas for higher B an increasing transition temperature was observed, see for example refs. [44–47]. In summary, in recent years the magnetic field-temperature phase diagram grew out to be a highly non-trivial testing ground for QCD models. The determination of additional details of this phase diagram — like the effect of changing the quark masses — will therefore further contribute to a better understanding of the limitations of such effective descriptions.

In this paper we will make a step towards a better understanding of this second issue. Our purpose is to study how the catalytic or anticatalytic effect of the magnetic field depends on the pion mass, or equivalently on the mass m of the light quarks, pinning down the limiting value at which IMC turns into MC. For each m, we do this at the corresponding critical temperature $T_c = T_c(m)$, and at a fixed value of the magnetic field in physical units. The dependence on the pion mass was also the subject of ref. [13]. Here

we employ a larger set of pion masses to follow more closely the transition from IMC to MC. Moreover, we employ a different, mass-independent scale-setting procedure to assess the robustness of the qualitative picture obtained in ref. [13] against different ways to build QCD for unphysical pion masses.

The plan of the paper is the following. In section 2 we give the details of our calculation, including the determination of T_c and setting of the physical scale. In section 3 we specify our observables. In section 4 we discuss our numerical results. Finally, in section 5 we draw our conclusions and show our prospects for the future.

2   Numerical setup and methods

We perform our numerical calculations on $N_s^3 \times N_t$ lattices using the tree-level Symanzik improved gauge action with three flavors of stout improved rooted staggered quarks. We fix the strange quark mass to its physical value and vary the light quark mass $m = m_{\mathrm{ud}}$ between its physical value and the strange quark mass, i.e., between the physical and the $N_f = 3$ flavor symmetric point, using the values $m/m_{\mathrm{phys}} \in \{1, 4, 8, 12, 16, 18, 20, 28.15\}$. The details of our lattice ensembles, the line of constant physics and the lattice scale $a(\beta)$ are described in refs. [7, 48, 49]. We adopt a mass-independent scale-setting scheme, using the results of ref. [49] for the lattice scale determined at the physical point. In order to estimate the size of finite-spacing effects in the scale setting, we have alternatively set the lattice spacing using the w_0 scale [50] computed in the $N_f = 3$ system, making use of the continuum value $w_0 = 0.153\,\mathrm{fm}$ [51]. Notice that both procedures rely on a mass-independent scale setting, and are expected to lead to the same continuum results. We remark furthermore that the lattice scale could also be set in a mass-dependent manner — this approach was followed in ref. [13], which employs w_0 at the physical point and assumes that it is independent of m. Since there is no preferred choice when dealing with physics off the real world, a comparison between different scale-setting procedures does not assess a systematic error, but rather the robustness of the resulting qualitative pictures. A comparison to the results of ref. [13] will be provided below.

For our analysis both zero-temperature runs as well as finite-temperature simulations were necessary. We generated $T \approx 0$ configurations at $B = 0$ using four different values of the gauge coupling β summarized in table 1. These configurations are used for the determination of the additive renormalization of the condensate and of the lattice scale. The finite-temperature simulations were performed at fixed lattice spatial volume and temporal extension ($N_s = 24$ and $N_t = 6$). This translates approximately to lattice spacings between $0.15\,\mathrm{fm}$ and $0.29\,\mathrm{fm}$ with our two-level stout improved action. All of our finite temperature simulation points are summarized on figure 1. For each ensemble we generated $\mathcal{O}\,(200)$ well thermalized configurations separated by 10 HMC trajectories. In the analysis we compute the statistical error by the bootstrap procedure with 2000 bootstrap samples. We are performing fully correlated fits when it is necessary.

To fulfill the periodic boundary conditions, we need to use a quantized magnetic flux N_b in our simulations. The quantization condition reads

$$(N_s a)^2 \cdot q_d B = 2\pi N_b, \quad N_b \in \mathbb{Z}, \quad 0 \le N_b < N_s^2\,, \tag{2.1}$$

β	N_s	N_t
3.450	24	32
3.555	24	32
3.625	28	40
3.670	32	48

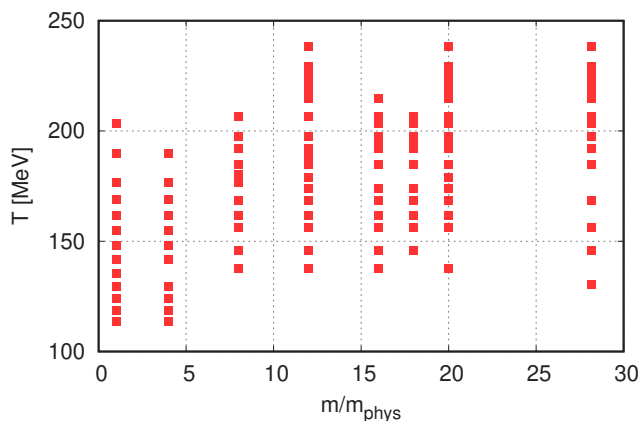**Table 1**. Bare parameters of our $T \approx 0$ ensembles.

Figure 1. The points on the $T - m$ plane used for configuration generation in this work.

where the smallest of the quark electric charges enters, that of the down quark $|q_d| = e/3$, with $e > 0$ being the elementary charge. In order to be able to resolve it, the magnetic field on our discretized lattice has to be very small in lattice units, i.e., $a^2 qB \ll 1$, which translates to $N_b/N_s^2 \ll 1$ in terms of the magnetic flux. In this work we use $N_b \in [11, 18]$, which results in $N_b/N_s^2 < 5\%$, thus in small discretization errors for B.

3 Observables

Our central observable is the light quark condensate $\langle \bar{\psi}\psi \rangle = \langle \bar{u}u + \bar{d}d \rangle / 2$. Here we follow the normalization introduced in ref. [8],

$$\Sigma(B, T, m) = \frac{2m_{\text{phys}}}{M_\pi^2 F^2} \left[\langle \bar{\psi}\psi \rangle_{B,T,m} - \langle \bar{\psi}\psi \rangle_{0,0,m} \right] + 1, \tag{3.1}$$

which contains the physical pion mass ($M_\pi = 135\,\text{MeV}$) and the chiral limit of the pion decay constant ($F = 86\,\text{MeV}$) at $B = 0$. The so defined combination is free of additive and multiplicative divergences and is normalized such that it equals unity for $T = B = 0$ and (according to leading-order chiral perturbation theory) approaches zero for high temperatures. Using eq. (3.1), the change of the condensate due to the magnetic field reads

$$\Delta\Sigma(B, T, m) = \Sigma(B, T, m) - \Sigma(0, T, m) = \frac{2m_{\text{phys}}}{M_\pi^2 F^2} \left[\langle \bar{\psi}\psi \rangle_{B,T,m} - \langle \bar{\psi}\psi \rangle_{0,T,m} \right]. \tag{3.2}$$

Note that here we take into account both (a) the sea effect by generating configurations at several values of the (quantized) magnetic flux, and (b) the valence effect by using the Dirac operator at $B > 0$ in the measurement.

Magnetic catalysis and inverse catalysis are distinguished by the sign of $\Delta\Sigma(B, T, m)$. Instead of mapping out the complete three-dimensional parameter space, in this work we concentrate on a one-dimensional subspace

$$\Delta\widetilde{\Sigma}(m) \equiv \Delta\Sigma(B_0, T_c(m, B = 0), m)\,. \tag{3.3}$$

Thus, we follow the line of pseudo-critical temperatures $T = T_c(m, B = 0)$ on the $T - m$ plane. Since at T_c the system is maximally sensitive to the fermionic determinant, in this way we expect anticatalytic effects to be at their strongest for each value of the light quark mass that we simulate. For the magnetic field we choose $eB_0 = 0.6\,\text{GeV}^2$, which is a typical value where the IMC phenomenon occurs [8]. On $N_t = 6$ lattices at the physical point, the system exhibits IMC, i.e. $\Delta\widetilde{\Sigma}(m_{\text{phys}}) < 0$, see ref. [8]. We will see below that increasing m increases $\Delta\widetilde{\Sigma}$, eventually turning it positive. The limiting quark mass $\widetilde{m}$ is defined implicitly by $\Delta\widetilde{\Sigma}(\widetilde{m}) = 0$.[1]

Besides the quark condensate, we also determined the average Polyakov loop, which has already been identified as the most relevant gluonic observable for the response of QCD matter to a background magnetic field [15]. It is defined as the average product of time-like links U_4 along a closed temporal loop of minimal length,

$$P = \frac{1}{V}\left\langle \sum_{\mathbf{x}} \text{Re}\,\text{Tr}\prod_{t=0}^{N_t-1} U_4(\mathbf{x}, t)\right\rangle. \tag{3.4}$$

We also consider the ratio

$$L_R = P(B, T, m)\big/P(0, T, m)\,, \tag{3.5}$$

in which the multiplicative divergences cancel (since those are independent of the magnetic field [15]).

4 Results

To determine $\widetilde{m}$, we first performed $B = 0$ simulations to calculate $T_c(m, B = 0)$ as a function of m. The pseudo-critical temperature was computed as the inflection point of $\Sigma(0, T, m)$, by means of an arctangent fit to the data, separately for each quark mass represented in figure 1. For illustration, we show in figure 2 our results for Σ at the three-flavor symmetric point with the arctan fits included. The two data sets correspond to two independent scale settings: (a) using f_K at the physical point [49], (b) using w_0 at the

---

[1]In general, the set $\Delta\Sigma(B, T, m) < 0$ is a domain in the $T - B$ plane for each value of the quark mass. For physical quark masses, $m = m_{\text{phys}}$, this domain includes the point $p = [eB = 0.6\text{ GeV}^2, T = T_c(m)]$. As the quark mass is increased, the domain shrinks. According to our definition, $\widetilde{m}$ is the limiting mass, where the point p crosses the border of the domain. Choosing p differently will change our result slightly but will not affect the emerging picture qualitatively.
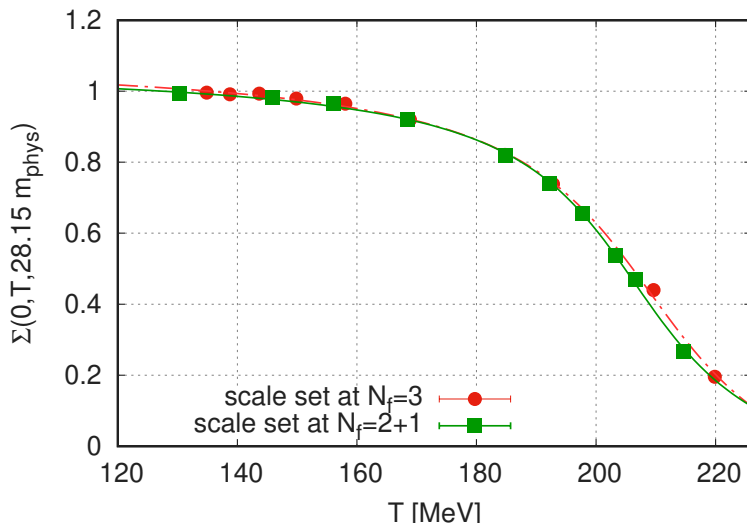
Figure 2. Comparison of the two scale setting procedures described in the text. Red circles indicate the results using the w_0 scale at the $N_f = 3$ point, while the green squares correspond to the $2 + 1$-flavor LCP [49].

$N_f = 3$ point. From the figure it is apparent that the uncertainty coming from the scale setting is tiny. This is also reflected by the extracted inflection points, which agree with each other within one standard deviation. At the physical point we find on our $N_t = 6$ lattices that $T_c\,(m_{\mathrm{phys}}, B = 0) = 149.9(9)\,\mathrm{MeV}$, only a few percent away from the continuum limit $T_c^{\mathrm{cont}} = 157(4)\,\mathrm{MeV}$ [52]. We take this as an indication of small finite-spacing effects.

From the $T_c(m)$ data we can determine the complete pseudo-critical trajectory using an interpolation in the quark mass. We have tried fits with several functional forms, namely the "rational" function

$$T_c(m) = T_c(0)\frac{1 + a\,m^c}{1 + b\,m^c}\,, \tag{4.1}$$

and the power-law behavior

$$T_c(m) = T_c(0) + am^u(1 + bm^2 + cm^4)\,, \tag{4.2}$$

where we set $u = \frac{1}{\beta\delta}$ with β and δ the critical exponents of the O(4) or the O(2) universality classes (see, e.g., ref. [53]). We plot our results in figure 3 against the respective pion masses (for their determination, see below), and list our resulting fit parameters in tables 2 and 3. The errors of $T_c(m)$ used in the fits include the statistical error and the systematic error related to the choice of fitting range in the determination of the inflection point. In the plot a further 2% uncertainty due to the determination of the physical scale (see ref. [52]) is also included.

In figure 3 we include also the results of the Pisa group (figure 6 of ref. [13]) for comparison. While the different scale-setting procedure obviously leads to quantitatively different results from ours, the qualitative behaviors match nicely.

As an interesting side result, we determine the critical temperature in the chiral limit as $T_c(m = 0) = 138(4)\,\mathrm{MeV}$. The central value is obtained averaging the three best fits in

	"rational"
$T_c(0)$ [MeV]	140(4)
a	0.17(4)
b	0.09(1)
c	0.8(2)
χ^2/d.o.f.	0.6

Table 2. The parameters of a fit to the $T_c(m)$ data using the function of eq. (4.1).

	O(4)	O(2)
$T_c(0)$ [MeV]	138(1)	135(1)
a [MeV]	12.2(5)	14.5(6)
b	$-6(1) \cdot 10^{-4}$	$-4(1) \cdot 10^{-4}$
c	$4(1) \cdot 10^{-7}$	$3(1) \cdot 10^{-7}$
χ^2/d.o.f.	0.4	0.4

Table 3. The parameters of a fit to the $T_c(m)$ data using the function of eq. (4.2), with u chosen according to the indicated critical behavior.
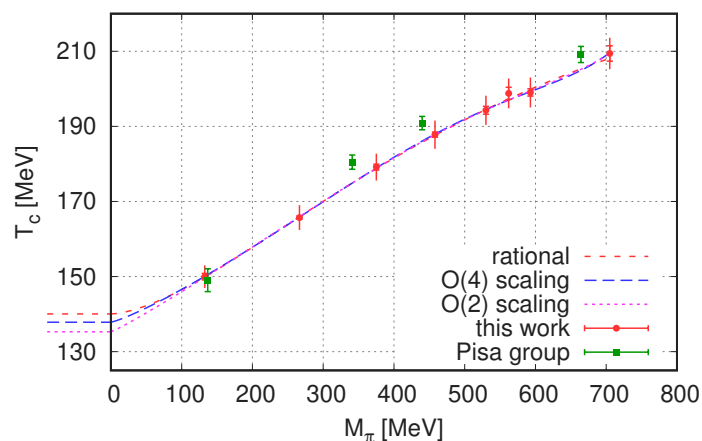
Figure 3. The pseudo-critical trajectory, together with the results of fits performed according to eqs. (4.1) and (4.2). The extended error bars include the systematic effect due to scale setting. Data from ref. [13] are also included for comparison.

tables 2 and 3, while the error is obtained by averaging in quadrature the corresponding statistical errors and the deviation of the three central values from the mean.

Due to the quantization condition, eq. (2.1), we are not able to perform simulations at the same physical magnetic field on all points of the pseudo-critical trajectory. In order to correct for this, we perform for each quark mass several simulations near $eB_0 = 0.6$ GeV^2 and $T_c(m)$ and interpolate linearly in the magnetic field and in the temperature. For illustration we show our results for the interpolation at a particular light quark mass on figure 4.
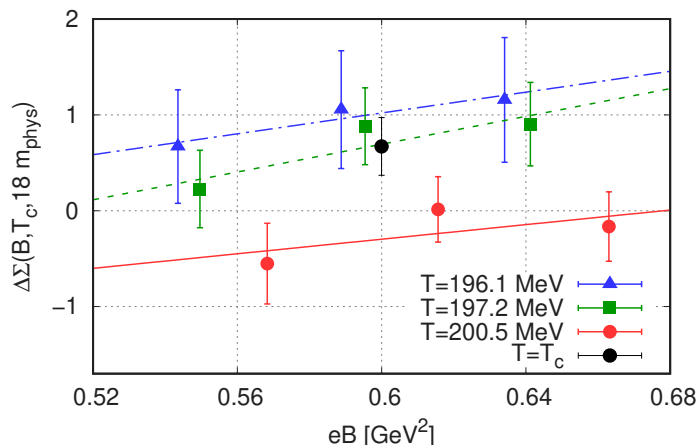
Figure 4. Visualization of our interpolation scheme for $m/m_{\mathrm{phys}} = 18$. The pseudo-critical temperature is $T_c = 197.3(5)$ MeV. The lines indicate the results of the interpolation in B to $eB_0 = 0.6\,\mathrm{GeV}^2$ at a fixed temperature, and the black filled circle represents the result of the final interpolation in the temperature.
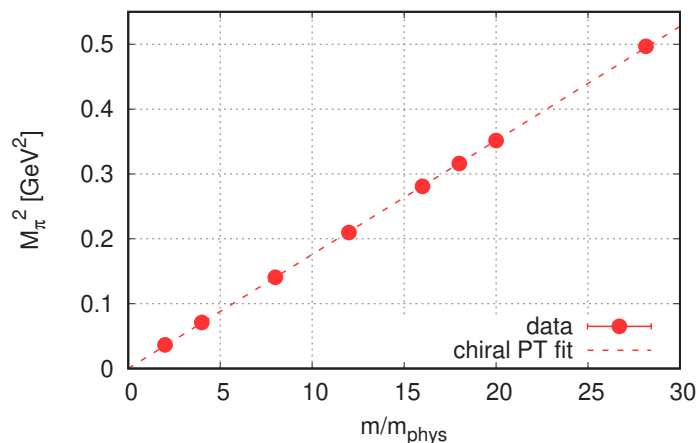

Figure 5. The squared pion mass as a function of the light quark mass. The dashed line indicates the linear dependence predicted by chiral perturbation theory.

In order to interpret our results in terms of physical parameters, we also determined the pion mass M_π using our zero temperature ensembles for several quark masses. We show our results in figure 5, which agree well with the prediction of chiral perturbation theory for the pion mass. We find $M_\pi^2 = M_0^2 \cdot (m/m_{\mathrm{phys}})$ with $M_0 = 132.62(4)\,\mathrm{MeV}$, in good agreement with the physical pion mass. This dependence is used to interpolate the pion mass for intermediate values of m.

The main result of this paper is shown in figure 6, where we plot the change of the renormalized chiral condensate $\Delta\widetilde{\Sigma}$ of eq. (3.3) against the quark mass (and, equivalently, against the pion mass). Remember that this quantity measures the change in the condensate when switching on a magnetic field of magnitude $eB_0 = 0.6\,\mathrm{GeV}^2$ at the pseudo-critical temperature $T_c(m)$. The sign of $\Delta\widetilde{\Sigma}$ changes from negative to positive at the limiting quark
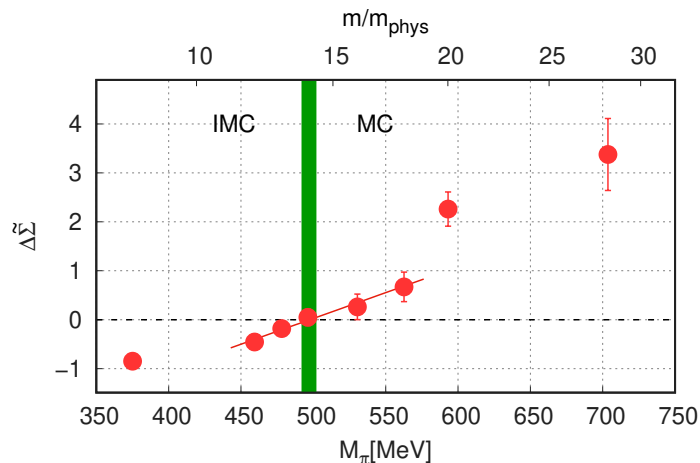
Figure 6. The change in the condensate due to the magnetic field $eB_0 = 0.6\,\mathrm{GeV}^2$ along the pseudo-critical trajectory in terms of the pion mass. The green vertical line indicates the limiting pion mass, which separates the IMC and MC regions.

mass $\widetilde{m} = 14.07(55)\,m_{\mathrm{phys}}$. The corresponding pion mass equals $\widetilde{M}_\pi = 497(4)\,\mathrm{MeV}$. We obtain this value using a linear interpolation in the interval $M_\pi \in [450, 570]\,\mathrm{MeV}$ with reduced $\chi^2 \simeq 1$. These results show that a change from IMC to MC in the response of strongly interacting matter to a background magnetic field takes place for sufficiently heavy pions, as already observed in ref. [13], and allow us to quantify how heavy pions have to be.

Finally, in figure 7 we show the Polyakov loop ratio (3.5), which clearly shows that the renormalized Polyakov loop increases monotonically for all quark masses in the transition region. This finding is in line with the recent results of ref. [13], where also the inflection point of P was determined and $T_c(B)$ was shown to be a decreasing function of B for pion masses up to $M_\pi \approx 660\,\mathrm{MeV}$, independently of whether MC or IMC takes place.[2] This can perhaps be understood in terms of the inverse correlation between the Polyakov loop and the reweighting factor of a gauge configuration due to switching on a magnetic field, observed in ref. [15]. Such a correlation implies that configurations with larger values of the average Polyakov loop are favored in the presence of a magnetic field, compared to the typical configurations at $B = 0$. This pushes the system towards the ordered phase, thus anticipating the transition and lowering the pseudocritical temperature for $B \neq 0$. Whether this leads to MC or IMC at T_c depends instead on the correlation between the chiral condensate and the reweighting factor. The results of ref. [13] and of this paper suggest that while there is always inverse correlation between the Polyakov loop and the reweighting factor, the sign of the correlation between the chiral condensate and the reweighting factor depends on the quark mass.

---

[2]The Polyakov loop is expected to be independent of the magnetic field both for sufficiently low and for sufficiently high temperatures. Thus, the implicit condition $P(T_c) = \mathrm{const.}$ is a feasible alternative definition for the transition temperature T_c. An increase in $P(B)$ for all temperatures therefore results in a decreasing $T_c(B)$. Note that an analogous construction does not capture the behavior of the quark condensate, since Σ depends on B even at $T = 0$.
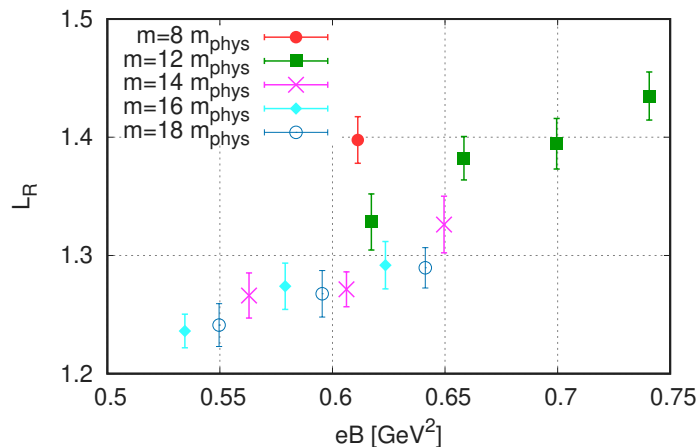
Figure 7. The Polyakov loop ratio (3.5) around the point where inverse magnetic catalysis turns into magnetic catalysis.

5 Conclusions

In this paper we have determined the limiting light quark mass (or equivalently the pion mass) above which QCD does not exhibit inverse magnetic catalysis anymore in the transition region. Specifically, we considered a fixed magnetic field $eB_0 = 0.6$ GeV^2 and evaluated the quark condensate along the pseudo-critical temperature trajectory $T_c(m, B = 0)$. This choice was made so that the sea effect due to the fermion determinant was as strong as possible. Our results agree with the general findings of the Pisa group, reported in ref. [13], namely that IMC turns into MC for large enough pion masses, and also allow to pinpoint the particular value at which this happens for our choice of magnetic field. In our setting, we found that the system turns from displaying IMC to MC at $M_\pi \approx 3.7 \cdot M_{\pi,\mathrm{phys}}$. This value is consistent with the results of ref. [13], although a quantitative comparison would require to take into account their use of a different scale-setting procedure. Our results are also consistent with the preliminary results reported in ref. [54]. The results of this paper were obtained at a single lattice spacing, but we found indications that finite-spacing effects are small. While an extrapolation to the continuum is expected to give (slightly) different quantitative results, we believe that the qualitative picture of a change from MC to IMC is robust. Being based on a first-principles calculation on the lattice, our results provide a nontrivial testing ground for effective models aiming at the description of the inverse magnetic catalysis phenomenon.

References

[1] E.S. Fraga, *Thermal chiral and deconfining transitions in the presence of a magnetic background*, *Lect. Notes Phys.* **871** (2013) 121 [`arXiv:1208.0917`] [ɪɴSPIRE].

[2] J.O. Andersen, W.R. Naylor and A. Tranberg, *Phase diagram of QCD in a magnetic field: A review*, *Rev. Mod. Phys.* **88** (2016) 025001 [`arXiv:1411.7176`] [ɪɴSPIRE].

[3] V.A. Miransky and I.A. Shovkovy, *Quantum field theory in a magnetic field: From quantum chromodynamics to graphene and Dirac semimetals*, *Phys. Rept.* **576** (2015) 1 [`arXiv:1503.00732`] [ɪɴSPIRE].

[4] D.E. Kharzeev, J. Liao, S.A. Voloshin and G. Wang, *Chiral magnetic and vortical effects in high-energy nuclear collisions — A status report*, *Prog. Part. Nucl. Phys.* **88** (2016) 1 [`arXiv:1511.04050`] [ɪɴSPIRE].

[5] I.A. Shovkovy, *Magnetic Catalysis: A Review*, *Lect. Notes Phys.* **871** (2013) 13 [`arXiv:1207.5081`] [ɪɴSPIRE].

[6] M. D'Elia, S. Mukherjee and F. Sanfilippo, *QCD Phase Transition in a Strong Magnetic Background*, *Phys. Rev.* **D 82** (2010) 051501 [`arXiv:1005.5365`] [ɪɴSPIRE].

[7] G.S. Bali et al., *The QCD phase diagram for external magnetic fields*, *JHEP* **02** (2012) 044 [`arXiv:1111.4956`] [ɪɴSPIRE].

[8] G.S. Bali, F. Bruckmann, G. Endrődi, Z. Fodor, S.D. Katz and A. Schäfer, *QCD quark condensate in external magnetic fields*, *Phys. Rev.* **D 86** (2012) 071502 [`arXiv:1206.4205`] [ɪɴSPIRE].

[9] G. Endrődi, *Critical point in the QCD phase diagram for extremely strong background magnetic fields*, *JHEP* **07** (2015) 173 [`arXiv:1504.08280`] [ɪɴSPIRE].

[10] E.M. Ilgenfritz, M. Müller-Preussker, B. Petersson and A. Schreiber, *Magnetic catalysis (and inverse catalysis) at finite temperature in two-color lattice QCD*, *Phys. Rev.* **D 89** (2014) 054512 [`arXiv:1310.7876`] [ɪɴSPIRE].

[11] V.G. Bornyakov, P.V. Buividovich, N. Cundy, O.A. Kochetkov and A. Schäfer, *Deconfinement transition in two-flavor lattice QCD with dynamical overlap fermions in an external magnetic field*, *Phys. Rev.* **D 90** (2014) 034501 [`arXiv:1312.5628`] [ɪɴSPIRE].

[12] G.S. Bali, F. Bruckmann, G. Endrődi, S.D. Katz and A. Schäfer, *The QCD equation of state in background magnetic fields*, *JHEP* **08** (2014) 177 [`arXiv:1406.0269`] [ɪɴSPIRE].

[13] M. D'Elia, F. Manigrasso, F. Negro and F. Sanfilippo, *QCD phase diagram in a magnetic background for different values of the pion mass*, *Phys. Rev.* **D 98** (2018) 054509 [`arXiv:1808.07008`] [ɪɴSPIRE].

[14] M. D'Elia and F. Negro, *Chiral Properties of Strong Interactions in a Magnetic Background*, *Phys. Rev.* **D 83** (2011) 114028 [`arXiv:1103.2080`] [ɪɴSPIRE].

[15] F. Bruckmann, G. Endrődi and T.G. Kovács, *Inverse magnetic catalysis and the Polyakov loop*, *JHEP* **04** (2013) 112 [`arXiv:1303.3972`] [ɪɴSPIRE].

[16] C. Bonati et al., *Magnetic field effects on the static quark potential at zero and finite temperature*, *Phys. Rev.* **D 94** (2016) 094007 [arXiv:1607.08160] [InSPIRE].

[17] V.P. Gusynin, V.A. Miransky and I.A. Shovkovy, *Dimensional reduction and catalysis of dynamical symmetry breaking by a magnetic field*, *Nucl. Phys.* **B 462** (1996) 249 [hep-ph/9509320] [InSPIRE].

[18] F. Bruckmann et al., *Landau levels in QCD*, *Phys. Rev.* **D 96** (2017) 074506 [arXiv:1705.10210] [InSPIRE].

[19] T. Kojo and N. Su, *The quark mass gap in a magnetic field*, *Phys. Lett.* **B 720** (2013) 192 [arXiv:1211.7318] [InSPIRE].

[20] E.S. Fraga and L.F. Palhares, *Deconfinement in the presence of a strong magnetic background: an exercise within the MIT bag model*, *Phys. Rev.* **D 86** (2012) 016008 [arXiv:1201.5881] [InSPIRE].

[21] K. Fukushima and Y. Hidaka, *Magnetic Catalysis Versus Magnetic Inhibition*, *Phys. Rev. Lett.* **110** (2013) 031601 [arXiv:1209.1319] [InSPIRE].

[22] E.S. Fraga, J. Noronha and L.F. Palhares, *Large N_c Deconfinement Transition in the Presence of a Magnetic Field*, *Phys. Rev.* **D 87** (2013) 114014 [arXiv:1207.7094] [InSPIRE].

[23] G. Endrődi, *QCD equation of state at nonzero magnetic fields in the Hadron Resonance Gas model*, *JHEP* **04** (2013) 023 [arXiv:1301.1307] [InSPIRE].

[24] J. Chao, P. Chu and M. Huang, *Inverse magnetic catalysis induced by sphalerons*, *Phys. Rev.* **D 88** (2013) 054009 [arXiv:1305.1100] [InSPIRE].

[25] K. Kamikado and T. Kanazawa, *Chiral dynamics in a magnetic field from the functional renormalization group*, *JHEP* **03** (2014) 009 [arXiv:1312.3124] [InSPIRE].

[26] E.J. Ferrer, V. de la Incera and X.J. Wen, *Quark Antiscreening at Strong Magnetic Field and Inverse Magnetic Catalysis*, *Phys. Rev.* **D 91** (2015) 054006 [arXiv:1407.3503] [InSPIRE].

[27] L. Yu, H. Liu and M. Huang, *Spontaneous generation of local CP-violation and inverse magnetic catalysis*, *Phys. Rev.* **D 90** (2014) 074009 [arXiv:1404.6969] [InSPIRE].

[28] N. Müller, J.A. Bonnet and C.S. Fischer, *Dynamical quark mass generation in a strong external magnetic field*, *Phys. Rev.* **D 89** (2014) 094023 [arXiv:1401.1647] [InSPIRE].

[29] S. Fayazbakhsh and N. Sadooghi, *Anomalous magnetic moment of hot quarks, inverse magnetic catalysis and reentrance of the chiral symmetry broken phase*, *Phys. Rev.* **D 90** (2014) 105030 [arXiv:1408.5457] [InSPIRE].

[30] R. Rougemont, R. Critelli and J. Noronha, *Holographic calculation of the QCD crossover temperature in a magnetic field*, *Phys. Rev.* **D 93** (2016) 045013 [arXiv:1505.07894] [InSPIRE].

[31] K.A. Mamo, *Inverse magnetic catalysis in holographic models of QCD*, *JHEP* **05** (2015) 121 [arXiv:1501.03262] [InSPIRE].

[32] D. Dudal, D.R. Granado and T.G. Mertens, *No inverse magnetic catalysis in the QCD hard and soft wall models*, *Phys. Rev.* **D 93** (2016) 125004 [arXiv:1511.04042] [InSPIRE].

[33] S. Mao, *Inverse magnetic catalysis in Nambu-Jona-Lasinio model beyond mean field*, *Phys. Lett.* **B 758** (2016) 195 [arXiv:1602.06503] [InSPIRE].

[34] N. Evans, C. Miller and M. Scott, *Inverse Magnetic Catalysis in Bottom-Up Holographic QCD*, *Phys. Rev.* **D 94** (2016) 074034 [arXiv:1604.06307] [InSPIRE].

[35] U. Gürsoy, I. Iatrakis, M. Järvinen and G. Nijs, *Inverse Magnetic Catalysis from improved Holographic QCD in the Veneziano limit*, *JHEP* **03** (2017) 053 [arXiv:1611.06339] [INSPIRE].

[36] V.P. Pagura, D. Gómez Dumm, S. Noguera and N.N. Scoccola, *Magnetic catalysis and inverse magnetic catalysis in nonlocal chiral quark models*, *Phys. Rev.* **D 95** (2017) 034013 [arXiv:1609.02025] [INSPIRE].

[37] D. Giataganas, U. Gürsoy and J.F. Pedraza, *Strongly-coupled anisotropic gauge theories and holography*, *Phys. Rev. Lett.* **121** (2018) 121601 [arXiv:1708.05691] [INSPIRE].

[38] U. Gürsoy, M. Järvinen, G. Nijs and J.F. Pedraza, *Inverse Anisotropic Catalysis in Holographic QCD*, *JHEP* **04** (2019) 071 [arXiv:1811.11724] [INSPIRE].

[39] D.M. Rodrigues, D. Li, E. Folco Capossoli and H. Boschi-Filho, *Chiral symmetry breaking and restoration in 2+1 dimensions from holography: Magnetic and inverse magnetic catalysis*, *Phys. Rev.* **D 98** (2018) 106007 [arXiv:1807.11822] [INSPIRE].

[40] R.L.S. Farias, K.P. Gomes, G.I. Krein and M.B. Pinto, *Importance of asymptotic freedom for the pseudocritical temperature in magnetized quark matter*, *Phys. Rev.* **C 90** (2014) 025203 [arXiv:1404.3931] [INSPIRE].

[41] M. Ferreira, P. Costa, O. Lourenço, T. Frederico and C. Providência, *Inverse magnetic catalysis in the (2+1)-flavor Nambu-Jona-Lasinio and Polyakov-Nambu-Jona-Lasinio models*, *Phys. Rev.* **D 89** (2014) 116011 [arXiv:1404.5577] [INSPIRE].

[42] A. Ayala, M. Loewe, A.J. Mizher and R. Zamora, *Inverse magnetic catalysis for the chiral transition induced by thermo-magnetic effects on the coupling constant*, *Phys. Rev.* **D 90** (2014) 036001 [arXiv:1406.3885] [INSPIRE].

[43] A. Ayala, M. Loewe and R. Zamora, *Inverse magnetic catalysis in the linear σ-model with quarks*, *Phys. Rev.* **D 91** (2015) 016002 [arXiv:1406.7408] [INSPIRE].

[44] E.S. Fraga, B.W. Mintz and J. Schaffner-Bielich, *A search for inverse magnetic catalysis in thermal quark-meson models*, *Phys. Lett.* **B 731** (2014) 154 [arXiv:1311.3964] [INSPIRE].

[45] J. Braun, W.A. Mian and S. Rechenberger, *Delayed Magnetic Catalysis*, *Phys. Lett.* **B 755** (2016) 265 [arXiv:1412.6025] [INSPIRE].

[46] J.O. Andersen, W.R. Naylor and A. Tranberg, *Inverse magnetic catalysis and regularization in the quark-meson model*, *JHEP* **02** (2015) 042 [arXiv:1410.5247] [INSPIRE].

[47] N. Müller and J.M. Pawlowski, *Magnetic catalysis and inverse magnetic catalysis in QCD*, *Phys. Rev.* **D 91** (2015) 116010 [arXiv:1502.08011] [INSPIRE].

[48] Y. Aoki, Z. Fodor, S.D. Katz and K.K. Szabó, *The Equation of state in lattice QCD: With physical quark masses towards the continuum limit*, *JHEP* **01** (2006) 089 [hep-lat/0510084] [INSPIRE].

[49] S. Borsányi et al., *The QCD equation of state with dynamical quarks*, *JHEP* **11** (2010) 077 [arXiv:1007.2580] [INSPIRE].

[50] S. Borsányi et al., *High-precision scale setting in lattice QCD*, *JHEP* **09** (2012) 010 [arXiv:1203.4469] [INSPIRE].

[51] S. Borsányi et al., *Calculation of the axion mass based on high-temperature lattice quantum chromodynamics*, *Nature* **539** (2016) 69 [arXiv:1606.07494] [INSPIRE].

[52] Y. Aoki et al., *The QCD transition temperature: results with physical masses in the continuum limit II.*, *JHEP* **06** (2009) 088 [arXiv:0903.4155] [INSPIRE].

[53] J. Engels, S. Holtmann, T. Mendes and T. Schulze, *Finite size scaling functions for 3-D O(4) and O(2) spin models and QCD*, *Phys. Lett.* **B 514** (2001) 299 [hep-lat/0105028] [INSPIRE].

[54] A. Tomiya, H.-T. Ding, X.-D. Wang, Y. Zhang, S. Mukherjee and C. Schmidt, *Phase structure of three flavor QCD in external magnetic fields using HISQ fermions*, PoS(LATTICE2018)163 (2019) [arXiv:1904.01276] [INSPIRE].